Atherosclerosis 235 (2014) 140–149

Contents lists available at ScienceDirect

Atherosclerosis

journal homepage: www.elsevier.com/locate/atherosclerosis

Coronary artery atherectomy reduces plaque shear strains: An endovascular elastography imaging study

Zahra Keshavarz-Motamed [a], Yoshifumi Saijo [b,c], Younes Majdouline [a], Laurent Riou [d], Jacques Ohayon [e,f], Guy Cloutier [a,g,*,1]

[a] Laboratory of Biorheology and Medical Ultrasonics, University of Montreal Hospital Research Center (CRCHUM), Montréal, Québec, Canada
[b] Graduate School of Biomedical Engineering, Tohoku University, Sendai, Japan
[c] Department of Cardiology, Tohoku University, Sendai, Japan
[d] INSERM, UMR_S 1039, Bioclinical Radiopharmaceutic, Faculty of Medicine, University Joseph-Fourier, Grenoble, France
[e] Laboratory TIMC-IMAG/DyCTiM, University Joseph-Fourier, CNRS UMR 5525, Grenoble, France
[f] University of Savoie, Polytech Annecy-Chambery, Le Bourget du Lac, France
[g] Department of Radiology, Radio-Oncology and Nuclear Medicine, and Institute of Biomedical Engineering, University of Montreal, Montréal, Québec, Canada

ARTICLE INFO

Article history:
Received 11 October 2013
Received in revised form
16 April 2014
Accepted 16 April 2014
Available online 30 April 2014

Keywords:
Vascular elastography
Vulnerable coronary atherosclerotic plaques
Shear strain imaging
Image processing
Intravascular ultrasound
Human study

ABSTRACT

Mechanical response and properties of the arterial wall can be used to identify the biomechanical instability of plaques and predict their vulnerability to rupture. Shear strain elastography (SSE) is proposed to identify vulnerable plaque features attributed to mechanical structural heterogeneities. The aims of this study were: 1) to report on the potential of SSE to identify atherosclerotic plaques; and 2) to use SSE maps to highlight biomechanical changes in lesion characteristics after directional coronary atherectomy (DCA) interventions. For this purpose, SSE was imaged using *in vivo* intravascular ultrasound (IVUS) radio-frequency data collected from 12 atherosclerotic patients before and after DCA intervention. Coronary atherosclerotic plaques (pre-DCA) showed high SSE magnitudes with large affected areas. There were good correlations between SSE levels and soft plaque content (*i.e.,* cellular fibrosis, thrombosis and fibrin) (mean |SSE| *vs.* soft plaque content: $r = 0.82$, $p < 0.01$). Significant differences were noticed between SSE images before and after DCA. Stable arteries (post-DCA) exhibited lower values than pre-DCA vessels (*e.g.,* pre-DCA: mean |SSE| = 3.9 ± 0.2% *vs.* 1.1 ± 0.2% post-DCA, $p < 0.001$). Furthermore, SSE magnitude was statistically higher in plaques with a high level of inflammation (*e.g.,* mean |SSE| had values of 4.8 ± 0.4% in plaques with high inflammation, whereas it was reduced to 1.8 ± 0.2% with no inflammation, $p < 0.01$). This study demonstrates the potential of the IVUS-based SSE technique to detect vulnerable plaques *in vivo*.

1. Introduction

Sudden death is the leading consequence of coronary artery disease in middle age and stands at the most dreadful end of the spectrum of acute coronary syndromes. In more than 50% of cases, the sudden death is related to an atherosclerotic plaque rupture [1]. The primary trigger for myocardial infarction is inflammatory-related biological destabilization of atherosclerotic plaques [2]. The prospective evaluation of the clinical success of a surgical intervention would benefit of an active identification of the rupture risk of detected lesions.

From autopsy studies in patients who had died of coronary artery diseases, the most common underlying plaque morphology was a ruptured thin-cap fibroatheroma (TCFA) with a superimposed thrombosis [3,4]. The TCFA is the precursor lesion that once ruptured, may lead to the formation of a thrombus causing an acute syndrome and possibly death [3]. Despite years of research on the subject, all biomechanical factors and mechanisms that make the vulnerable plaque (VP) susceptible to rupture are still not confidently known. However, it is generally believed that a large lipid pool, a thin fibrous cap (<100 μm), a high content of

* Corresponding author. Laboratory of Biorheology and Medical Ultrasonics, University of Montreal Hospital Research Center (CRCHUM), Room R11-464, Tour Viger, 900 rue Saint-Denis, Montréal, QC, Canada H2X 0A9. Tel.: +1 514 890 8000x24703.
E-mail address: guy.cloutier@umontreal.ca (G. Cloutier).
[1] Web: www.lbum-crchum.com.

http://dx.doi.org/10.1016/j.atherosclerosis.2014.04.022
0021-9150/

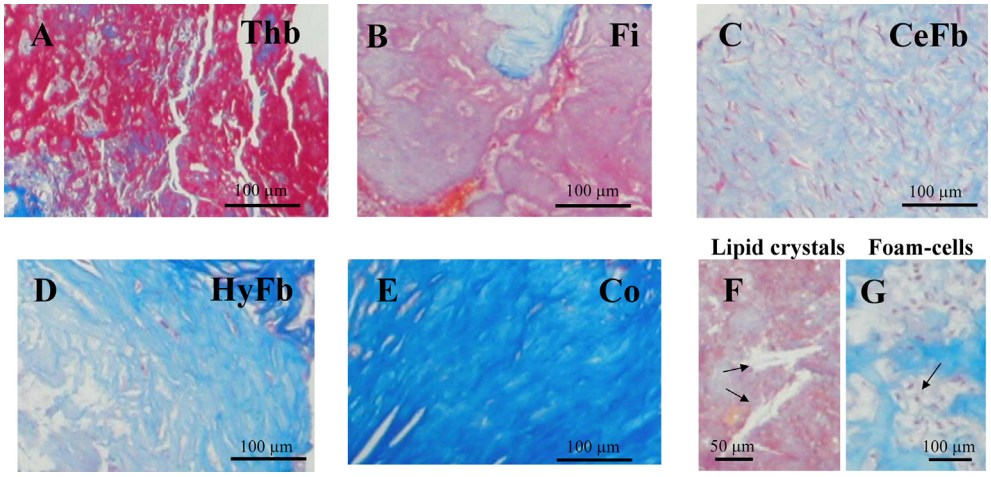

Fig. 1. Images showing morphologically distinguishable subtypes of atherosclerotic plaque constituents. A) Thrombotic (Thb) region. B) Fibrin (Fi) region. C) Cellular fibrous (CeFb) region. D) Hypocellular fibrous (HyFb) region. E) Collagen (Co) region. F) Lipid crystals (arrows). G) Macrophage-derived foam-cells (arrow). See text for detailed description.

inflammatory cells and a scarcity of smooth muscle cells are main contributors of plaque vulnerability [5].

Intravascular ultrasound (IVUS), optical coherence tomography, computed X-ray tomography and magnetic resonance imaging currently provide promising biomarkers because of their ability to detect plaques [4,6–12]. However, since morphological features are insufficient predictors of risks [13,14], prospective prediction of plaque rupture is still imprecise. Therefore, there is a need for a precise characterization of mechanical properties of plaque components [15]. In this context, several IVUS-based technologies were developed for the evaluation of vessel lesion characteristics and for therapy planning, namely endovascular elastography (EVE) [16,17], palpography [18,19] and virtual histology [20,21]. However, these technologies later became controversial and failed to properly quantify plaque mechanical and compositional properties [22–26].

From a biomechanical point of view, elevated shear strain is increasingly being considered to be an important factor for initiating and/or stimulating the development of a plaque into a rupture prone one by cap weakening leading to ulceration [27–29]. According to [28], the shear strain induced in the adventitial layer by the axial movement of the artery may promote vasa vasorum neovascularization, which in turn may lead to plaque progression by intraplaque inflammation and bleeding. In addition, Lawrence-Brown et al. [30] hypothesized that shear stresses could cause repeated intramural micro hemorrhages followed by a healing process leading to accelerated plaque development. Indeed,

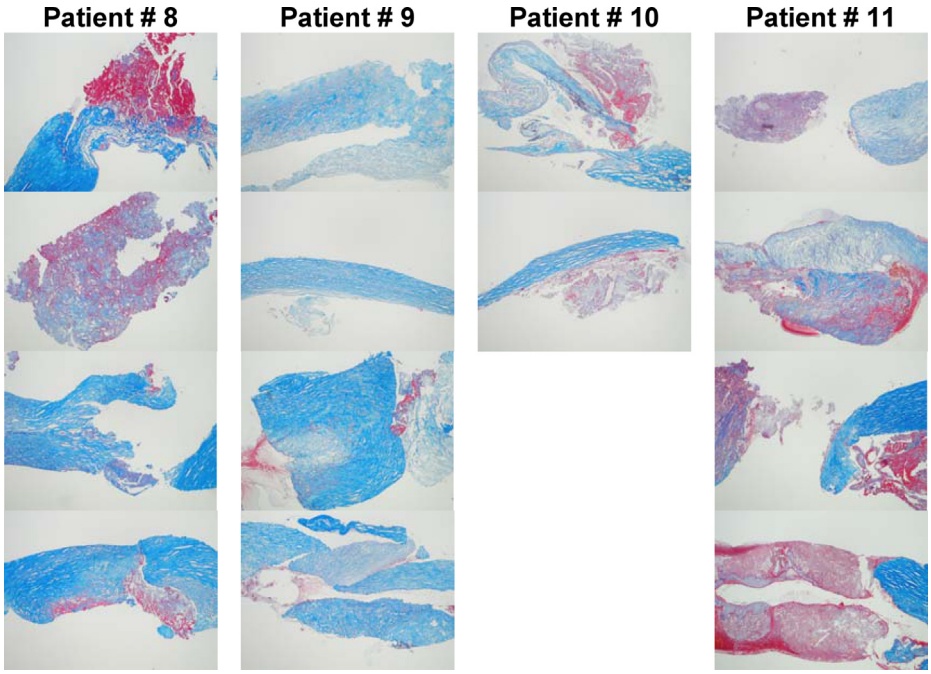

Fig. 2. Examples of microscopic histology stained samples for patients #8 – 11. The Elastica-Masson's trichrome (EMT) staining was used to characterize the composition of the atherosclerotic excised lesions, as shown in Fig. 1.

Table 1
Excised lesion compositions, from histological analysis performed by biologists, expressed as percent of total plaque area.

Patient number	Histology measurements (%)				
	Thrombosis	Fibrin	Cellular fibrosis	Hypocellular fibrosis	Collagen
1	0	11	37	10	42
2	0	5	63	32	0
3	0	13	45	21	21
4	13	27	30	15	15
5	0	15	68	3	14
6	6	35	23	5	31
7	0	10	51	23	16
8	9	34	26	2	29
9	0	9	45	7	39
10	0	43	16	15	26
11	14	40	18	12	16
12	9	10	25	3	53
Mean ± SD	**4.2 ± 5.4**	**21.0 ± 13.2**	**37.2 ± 16.5**	**12.3 ± 8.9**	**25.2 ± 14.0**

Soft plaque content

stiffness differences in plaque components may change structural shear stresses [31] and thus shear strains. This may lead to shear failure at the interface of tissue components with different stiffnesses [32,33]. Identifying shear strain within the arterial wall with imaging methods, therefore, should improve our ability to detect early functional abnormalities and may become a potential quantity to provide risk assessment of plaque vulnerability.

In the context of EVE imaging over cross-sections of an artery, early technical advances relied on the intraplaque radial [34,35] and circumferential [36,37] strain estimates. As a response to this need, we developed EVE based on the Lagrangian Speckle Model Estimator (LSME) [38] to estimate shear strain elastograms (SSE) [39]. In the latter study, this new development was validated against *in vitro* data acquired on polyvinyl alcohol cryogel vessel phantoms using standard finite element simulations. The potential of the SSE method to localize and identify vulnerable plaque features was also performed by applying it to *in vivo* data in atherosclerotic and diabetic pigs [39,40].

The aims of the present work were, therefore, 1) to study the potential of SSE to identify atherosclerotic plaques, and 2) to highlight the potential of SSE to investigate the evolution of mechanical properties following therapy and thus, the instability of atherosclerotic plaques. For this purpose, SSE maps were estimated by processing *in vivo* IVUS radio-frequency data collected from 12 atherosclerotic patients before and after directional coronary atherectomy (DCA) interventions. This pilot study demonstrates a reduction in magnitude of the shear strain field following DCA and thus the potential of the SSE-LSME technique to detect and characterize vulnerable plaques *in vivo*.

2. Materials and methods

2.1. Clinical data

Twelve patients (including two no re-flow cases and one perforation case) were studied under a research protocol approved by the Review Ethical Committee of Sendai University, Miyagi Social Insurance Hospital [41,42].

Before DCA, routine IVUS observations (Galaxy II® echograph, Boston Scientific, Natick, MA, USA, 40 MHz mechanically rotating probes) and radio-frequency (RF) signal acquisitions were

Table 2
Systemic pressure, level of inflammation (0: no inflammation, 1: medium level, 2: high level), and calcium detection (0: absence of calcium, 1: presence) for each patient.

Patient no.	Pressure (mmHg)	Inflammation level	Calcium detection
1	138/80	0	0
2	124/68	1	0
3	132/80	0	0
4	158/88	0	0
5	142/78	2	0
6	152/92	2	0
7	138/82	0	0
8	114/76	2	1
9	162/94	0	0
10	128/74	1	1
11	168/94	2	1
12	132/88	0	0

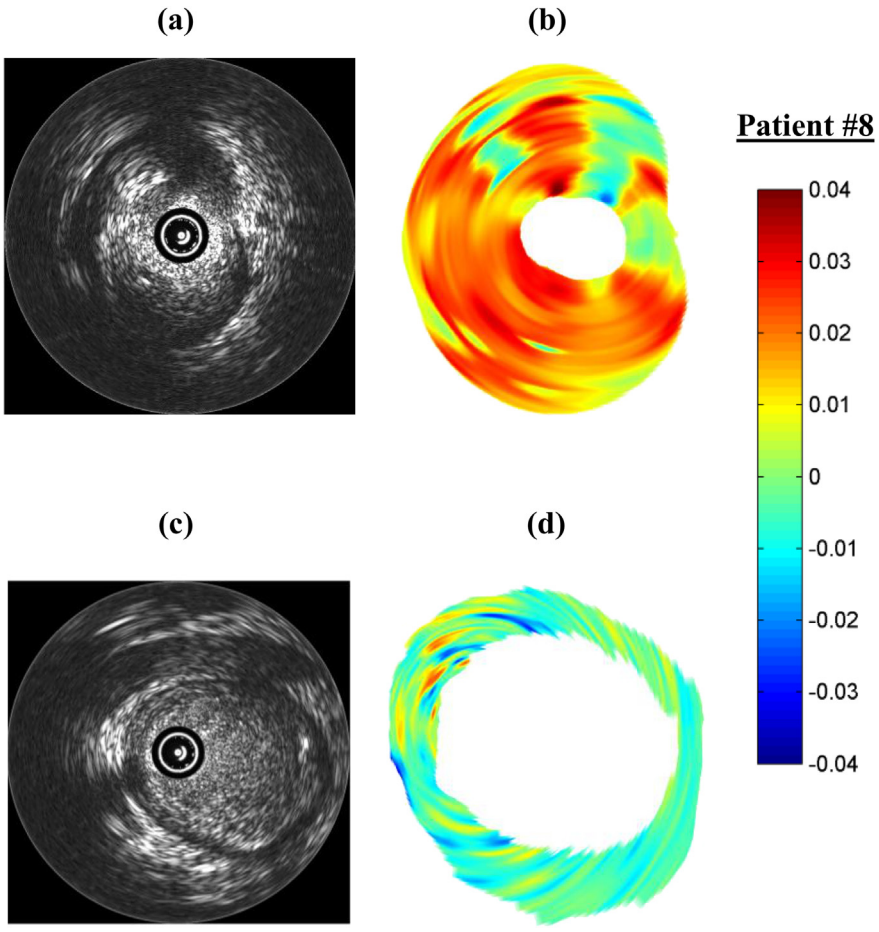

Fig. 3. Evolutions of estimated SSE before and after directional coronary atherectomy (DCA) for patient #8, (a) pre-DCA *in vivo* intravascular ultrasound (IVUS) image, (b) pre-DCA estimated SSE map, (c) post-DCA *in vivo* IVUS image, (d) post-DCA estimated SSE map. The color bar indicates the magnitude of SSE (multiply by 100 for values in percent). The SSE maps (second column) were calculated with IVUS RF data. For visualization purpose, SSE maps were zoomed in so they have different dimension scales compared with their respecting IVUS images. Pre-DCA: mean |SSE| (absolute value of SSE): 0.029, max |SSE|: 0.051; post-DCA: mean |SSE|: 0.01, max |SSE|: 0.021. (For interpretation of the references to color in this figure legend, the reader is referred to the web version of this article.)

performed. RF signals were digitized with a CS8500 8-bits 500 MHz acquisition card (GAGE, Lockport, IL, USA). For each patient, at a fixed axial catheter location to image the same atherosclerotic cross section during the cardiac cycle, a sequence of 30 images (at a frame rate of 30 images/s) was acquired. IVUS scanning was performed at the maximum stenosis site for all patients (*i.e.*, the cross-section with the smallest vessel lumen).

After DCA, another IVUS scan with RF data acquisition was performed at approximately the same axial position for a given patient. Because the DCA procedure removed most of the lesion, it was difficult to scan exactly the same ROI (region of interest) as pre-intervention. In order to keep the scan location as close as possible between pre- and post-DCA, the interventional cardiologist recorded the distance of the IVUS scan location from the closest upstream coronary bifurcation branch by measuring the time of auto pull-back under angiography guidance. Regarding the clockwise rotation in the IVUS image, the cardiologist marked the orifice of small side branches. He first performed a test cut so as to confirm the location and do the main cut by comparing the images.

2.2. Histology study on excised DCA lesions

Patients underwent a DCA procedure in which the atherosclerotic plaque was excised with a Flexicut catheter (Guidant Corporation, Santa Clara, CA, USA). Excised specimens were fixed in 10% formalin, embedded in paraffin using standard protocols, and then used to obtain 4-μm thick slices ($n = 2–4$/patient) with a microtome. The DCA procedure inherently leads to fragmentation and homogenization of excised atherosclerotic lesions. This implies that the overall *in situ* morphology of lesions cannot be inferred from coronary plaque specimens retrieved from the DCA procedure. In accordance with previously published studies [43,44], we assumed that the histological analysis of 2–4 slices, obtained from paraffin-embedded samples retrieved from the DCA procedure, allows one to have a representative view of the overall composition of the excised lesion. Histology analysis was performed using Elastica-Masson's trichrome (EMT) and CD68 immunochemical staining. Based on EMT staining, excised atherosclerotic lesions were subdivided into distinct components (Fig. 1). The thrombotic (Thb) and the fibrin (Fi) regions consisted of high density of red blood cells and fibrin, respectively; the cellular fibrous (CeFb) region included smooth muscle cells or other cells admixed with a low collagen content or elastic fiber; the hypocellular fibrous (HyFb) region contained extracellular connective tissue matrix with collagen and few cells; and the collagen (Co) region was defined as the site with a high density of collagen fibers. The intensity of the blue staining color revealed the amount of collagen content (strong blue indicates sites with high collagen content while light blue or no blue corresponds to sites with low collagen content). The area occupied by each component (thrombosis, fibrin, cellular fibrosis, hypocellular fibrosis and collagen; see Table 1) was determined on each of the 2–4 slices and the total area occupied by a given constituent

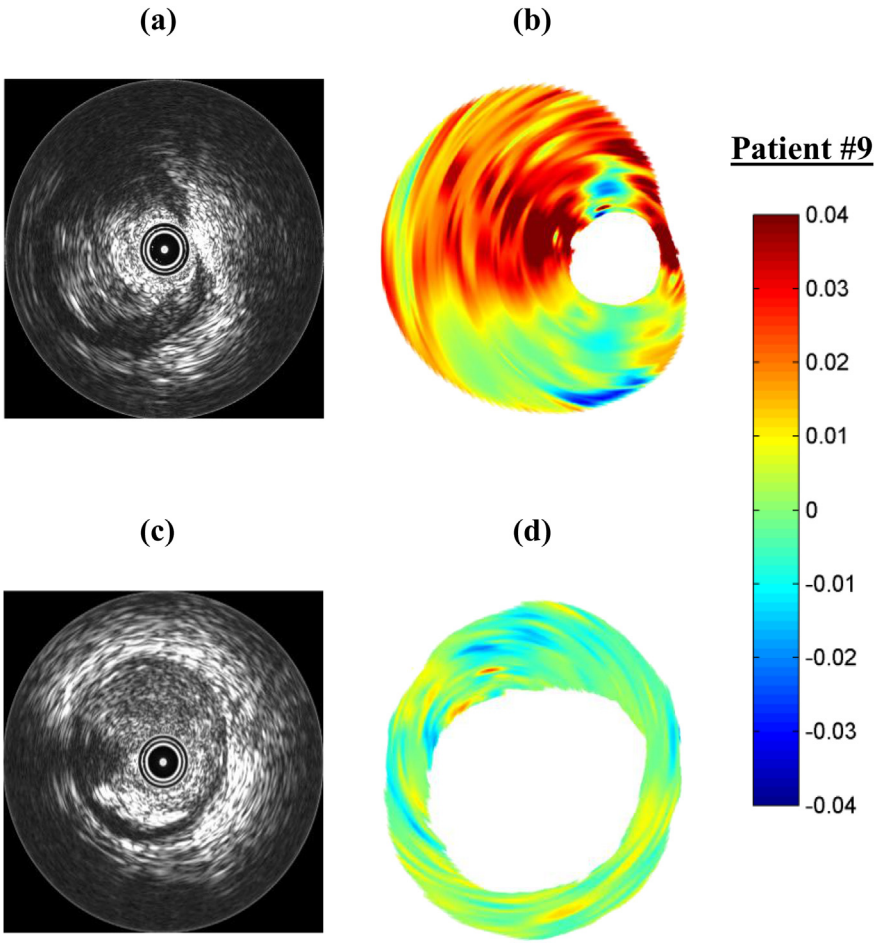

Fig. 4. Evolutions of estimated SSE before and after directional coronary atherectomy (DCA) for patient #9, (a) pre-DCA *in vivo* intravascular ultrasound (IVUS) image, (b) pre-DCA estimated SSE map, (c) post-DCA *in vivo* IVUS image, (d) post-DCA estimated SSE map. The color bar indicates the magnitude of SSE (multiply by 100 for values in percent). The SSE maps (second column) were calculated with IVUS RF data. For visualization purpose, SSE maps were zoomed in so they have different dimension scales compared with their respecting IVUS images. Pre-DCA: mean |SSE| (absolute value of SSE): 0.039, max |SSE|: 0.062; post-DCA: mean |SSE|: 0.014, max |SSE|: 0.021. (For interpretation of the references to color in this figure legend, the reader is referred to the web version of this article.)

was obtained by summing areas found on each slice using ImageJ software and color segmentation (ImageJ, NIH, Bethesda, MD, USA). This was done fully automatically with fixed threshold values to prevent any user bias. In each patient, the total lesion area being analyzed was also determined by summation of total areas of each of the 2–4 slices. The proportion of each component was determined as the ratio of the total area occupied by a given constituent to the total lesion area being analyzed. Lipid-rich regions could not be identified because of detachment during atherectomy and lipid removal over the process of tissue fixation and staining. However, the presence of macrophage-derived foam-cells and lipid crystals was analyzed. Representative microscopic histology stained samples are given in Fig. 2.

From this histological analysis performed by biologists, atherosclerotic lesions were subdivided in two groups. Soft plaque areas were considered to be regions with low-collagen components including thrombosis, fibrin and cellular fibrosis, whereas hypocellular fibrosis and collagen areas were considered stiffer, in agreement with previous published studies performed in both mouse and human [45–49]. Excised specimens were also semi-quantitatively analyzed for the presence of macrophages through CD68 immunochemical staining (0 = no, 1 = moderate and 2 = high inflammation; see Table 2). Table 2 also gives systolic/diastolic pressures of every patient pre-DCA, and detection of calcium on histology slices (0 = no calcium, 1 = calcium detected).

2.3. Plaque shear strain reconstruction

2.3.1. Image segmentation

IVUS images were segmented to detect the lumen and adventitia boundaries using a fast-marching model combining region and contour information [50]. Resulted contours were validated by a cardiologist (YS) before performing further processing. Pre-DCA, analyses were done on the ROI corresponding to the plaque burden (*i.e.*, the area between the lumen and adventitia boundaries). Post-DCA, the ROI represented the treated artery wall.

2.3.2. LSME elastography algorithm

RF image processing on detected ROIs was done with the Lagrangian Speckle Model Estimator (LSME) [38]. We used a developed version of this algorithm to calculate shear strain elastograms in polar coordinates with artifact corrections in cases of catheter eccentricity within the vessel lumen [39]. A brief summary of the algorithm is given in Appendix.

2.4. Correlation between SSE maps and histology study on excised DCA lesions

To investigate the correlation between SSE maps and excised lesion components, pre- and post-DCA elastograms (*i.e.*, mean and

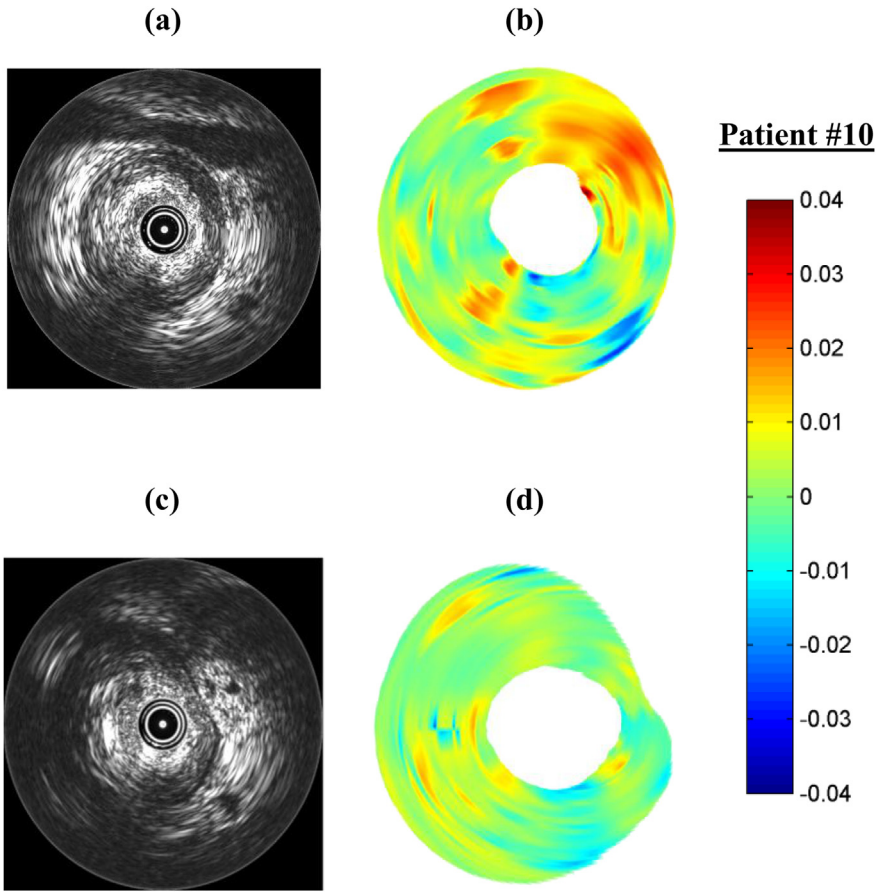

Fig. 5. Evolutions of estimated SSE before and after directional coronary atherectomy (DCA) for patient #10, (a) pre-DCA *in vivo* intravascular ultrasound (IVUS) image, (b) pre-DCA estimated SSE map, (c) post-DCA *in vivo* IVUS image, (d) post-DCA estimated SSE map. The color bar indicates the magnitude of SSE (multiply by 100 for values in percent). The SSE maps (second column) were calculated with IVUS RF data. For visualization purpose, SSE maps were zoomed in so they have different dimension scales compared with their respecting IVUS images. Pre-DCA: mean |SSE| (absolute value of SSE): 0.022, max |SSE|: 0.050; post-DCA: mean |SSE|: 0.0079, max |SSE|: 0.019. (For interpretation of the references to color in this figure legend, the reader is referred to the web version of this article.)

maximum absolute values of shear strains labeled mean |SSE| and max |SSE|) were compared with relative areas of soft plaque components over the entire vessel-wall cross sections. More specifically, the soft plaque areas were considered to be regions with low-collagen constituents including thrombosis, fibrin and cellular fibrosis (see Table 1).

2.5. Statistical analyses

Results were expressed as mean ± standard deviation (SD). Statistical analyses were performed with the SigmaStat software (version 3.1, Systat Software, San Jose, CA, USA). Analyses of variance (ANOVA) were used to detect any significant relation between SSE magnitude and plaque components or inflammation status. Association and agreement between variables were assessed by Pearson's correlations.

3. Results

3.1. The magnitude of SSE decreases post-DCA

Figs. 3 to 6 reveal differences between estimated SSE maps before and after DCA in few typical examples. Pre-atherectomy, intensified SSE magnitudes in large affected areas can be noticed. Regions of high SSE values in coronaries with atherosclerotic plaques are located, for these examples, between 5 and 10 o'clock in patient #8, between 9 and 2 o'clock in patients #9 and #11, and between 12 and 3 o'clock in patient #10 (Figs. 3b–6b). Post-atherectomy, stable arteries typically displayed low SSE magnitudes (Figs. 3c–6c). Post DCA, both mean and maximum |SSE| (*i.e.*, absolute values of SSE) showed significant reductions from 3.9 ± 0.2% and 5.7 ± 0.4% pre-DCA, to 1.1 ± 0.2% and 1.9 ± 0.1%, respectively (see Table 3). Reported values were computed over the entire vessel-wall cross section (*i.e.*, ROI) defined with detected lumen and adventitia boundaries.

3.2. The magnitude of SSE increases with soft plaque content

According to histology, all excised lesions had significant proportions of cellular fibrosis, collagen and fibrin (mean values: 37.2 ± 16.5%, 25.2 ± 14.0% and 21.0 ± 13.2%, respectively). Relative areas of hypocellular fibrosis and thrombosis were lower with mean values of 12.3 ± 8.9% and 4.2 ± 5.4%, respectively (Table 1). Non-significant proportions of calcified inclusions (less than 1%) were present in 3/12 samples. Table 2 summarizes our observations in this regard. As reported in Fig. 7a (pre-DCA), strong correlations were noticed between soft plaque content (*i.e.*, cellular fibrosis, thrombosis and fibrin) and mean (or maximum) |SSE| computed over the entire vessel-wall cross section: $r = 0.82$, $p < 0.01$ for mean |SSE|, and $r = 0.88$, $p < 0.01$ for max |SSE|. Moreover, strong correlations were still observed between soft plaque content and the

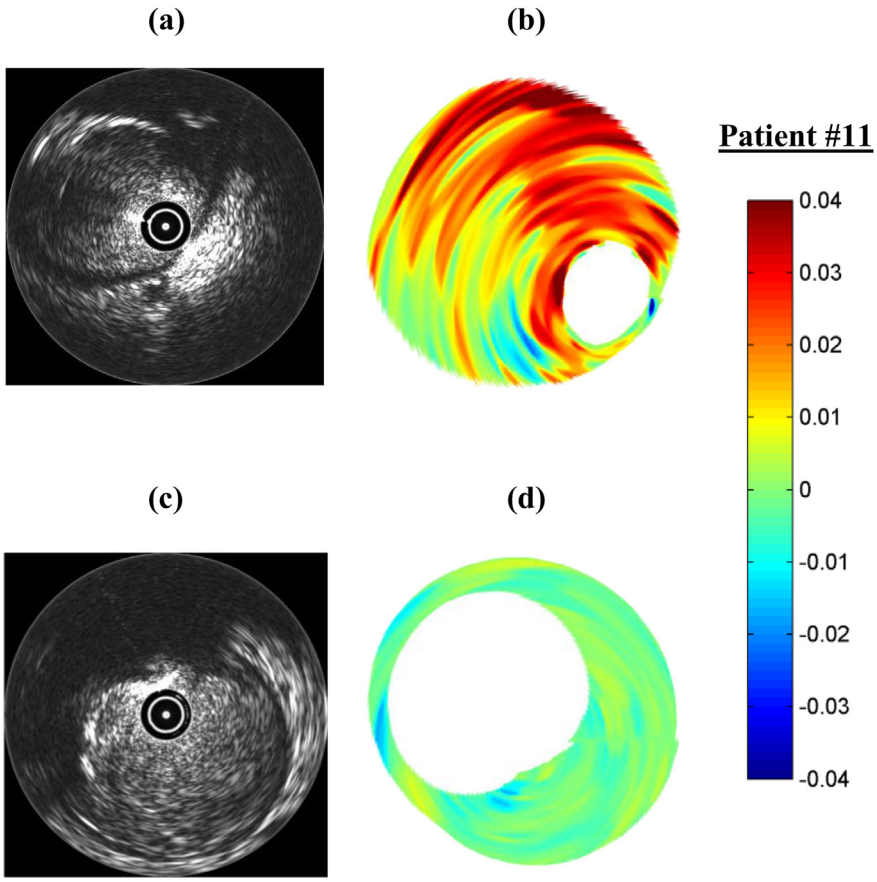

Fig. 6. Evolutions of estimated SSE before and after directional coronary atherectomy (DCA) for patient #11, (a) pre-DCA *in vivo* intravascular ultrasound (IVUS) image, (b) pre-DCA estimated SSE map, (c) post-DCA *in vivo* IVUS image, (d) post-DCA estimated SSE map. The color bar indicates the magnitude of SSE (multiply by 100 for values in percent). The SSE maps (second column) were calculated with IVUS RF data. For visualization purpose, SSE maps were zoomed in so they have different dimension scales compared with their respecting IVUS images. Pre-DCA: mean |SSE| (absolute value of SSE): 0.036, max |SSE|: 0.058; post-DCA: mean |SSE|: 0.013, max |SSE|: 0.020. (For interpretation of the references to color in this figure legend, the reader is referred to the web version of this article.)

difference of pre- and post-DCA |SSE| (mean |SSE|: $r = 0.88$, $p < 0.01$; max |SSE|: $r = 0.92$, $p < 0.01$).

3.3. The magnitude of SSE increases with plaque inflammation

Table 4 illustrates the correspondence between the inflammation status and SSE values. The worse was the inflammation status the higher were mean and max |SSE|. For example, the mean |SSE| had values of 1.8 ± 0.2% with no inflammation, and higher magnitudes of 3.1 ± 0.2% and 4.8 ± 0.4% for medium and high inflammation, respectively.

4. Discussions

Many strategies aimed to diagnose patients at risk of plaque rupture [51–53], though available screening and diagnostic methods are insufficient to identify victims before the clinical event occurs. There is, therefore, considerable demand for diagnosis and treatment of pathologic conditions that underlie sudden cardiac events [5].

As introduced earlier, there are evidence supporting the hypothesis that elevated shear strain initiates and/or stimulates the development of a plaque into a rupture prone one [27–29]. The accurate estimation of the shear strain is also imperative for accurate quantification of both the morphology and mechanical properties of the diseased artery at any given instant of the remodeling process. The morphology and mechanical properties are crucial for the prediction of plaque rupture [15,54] and such information may also lead to the development of specific therapies for the prevention of acute coronary events.

The following important findings can be deduced from results obtained in this study:

1) It is known that plaque instability at the cellular level is driven by factors such as inflammation, reduced collagen synthesis, local over expression of collagenase and smooth muscle cell apoptosis [2,32,55], altering mechanical properties of the plaque surface [56]. Inflammation has a central role in the pathogenesis of atherosclerosis and greatly influences the collagen composition of the plaque [57–60]. This made active inflammation as one of the major criteria for detection of vulnerable plaques [5]. In fact, inflammatory cells in the cap overlying the atheromatous

Table 3
Correlation analyses between estimated SSE and atherosclerotic plaque status.

	Mean |SSE| in % (mean ± SD)	Max |SSE| in % (mean ± SD)
Pre-DCA ($n = 12$)	3.9 ± 0.2 ($N = 7$) (§: $p < 0.001$)	5.7 ± 0.4 ($N = 7$) (§: $p < 0.01$)
Post-DCA ($n = 12$)	1.1 ± 0.2 ($N = 6$)	1.9 ± 0.1 ($N = 6$)

§: compared with post-DCA status.
N: required minimum population of patients for a 95% of confidence.

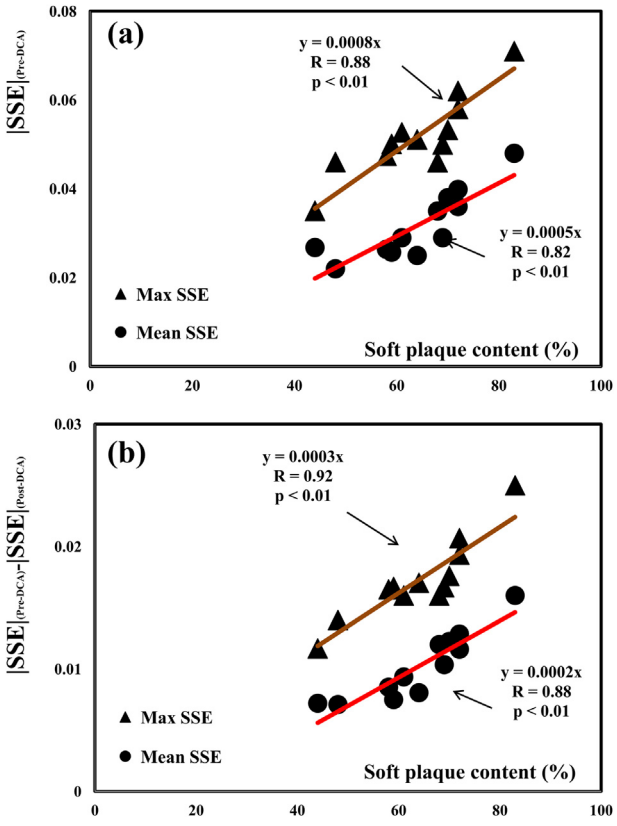

Fig. 7. Correlation analyses between mean and max |SSE| and soft plaque content (expressed as percent of the total excised plaque area). Multiply the *y*-axis by 100 for SSE values in percent. (a) Pre-DCA, (b) Difference of pre- and post-DCA.

core modulate collagen synthesis by positive and negative growth factors [60]. Metalloproteinases derived from activated macrophages also degrade collagen through the effect of inflammation [60]. We noticed, in this study, significant correlations between plaque SSE magnitudes, and the level of inflammation and soft plaque content, respectively. SSE, therefore, may detect the effect of these two interrelated cellular mechanisms influencing the mechanical stability of the plaque. This correspondence needs to be further investigated with larger sample sizes in humans.

2) Results of the current study revealed that areas with elevated SSE may correspond to soft and potentially vulnerable plaques. Indeed, stable arteries (post-DCA) exhibited significantly lower values than pre-DCA arteries, without any region of elevated SSE. Unfortunately, our data did not allow assessing the comparison between healthy tissues and SSE maps since we did not record any IVUS RF sequences in the healthy part of coronaries. However, in a recent study, the estimated SSE maps calculated from *in vivo* RF data were compared with histological observations in carotid plaques of atherosclerotic pigs [39]. In that study, we observed that all plaques were characterized by high magnitudes in SSE maps that correlated with American Heart Association atherosclerosis stage classifications. Also, normal parts of vascular walls (parts without any pathologic lesion) typically displayed low SSE values [39]. Therefore, the SSE-enabled LSME imaging technique may have the potential to localize and identify vulnerable plaque features *in vivo*.

4.1. Soft plaque characterization

This study reported SSE magnitudes as a function of soft plaque content. Percentages of soft plaque with respect to whole histology sections were defined as the amount of cellular fibrosis, thrombosis and fibrin. Ultrasound images acquired at the site of minimum cross-sectional lumen area were used to ensure that SSE map assessment was performed at the site where most atherosclerotic tissues would next be excised over the course of the DCA procedure. Thereby, the assumption that the histological analysis of fragmented and homogenized coronary plaque specimens from DCA is representative of the overall composition of the excised lesion seemed supported by results of Fig. 7, despite the unavoidable difficult morphometric matching between pre-DCA and post-DCA IVUS scans, and *in vitro* histological slices.

Our group [48] recently described the elastic material properties of mouse atherosclerotic lesion components. We found that hypocellular fibrotic areas were stiffer than cellular fibrotic zones. These results were partially confirmed a few months later by Hayenga et al. [49] on a similar experimental model. Importantly, similar findings were obtained earlier from human tissues by Lee et al. [45], Loree et al. [46], and Williamson et al. [47]. As observed in mice, these studies demonstrated that the stiffness of hypocellular fibrotic areas is greater than that of cellular areas. The analysis of the present study allowed identification of cellular nuclei (through Elastica-Masson's trichrome staining) and macrophages. Both of these were classified as pertaining to the cellular fibrotic zone and therefore were qualified to be considered as soft constituents of atherosclerotic lesions.

4.2. Potential clinical implications

The data presented in this study were based on a rather small population with data acquired in twelve patients. However, the aforementioned results explored that shear strain elastography, which is a new IVUS imaging modality, may appear promising to detect atherosclerotic plaques and assess their vulnerabilities before they become unstable. The ability of this method to monitor evolutions of a plaque and its response to therapies was substantiated by the observation of the reduction in SSE magnitudes post-atherectomy. More specifically, the followings can be considered:

Table 4
Correlation analyses between estimated SSE and inflammation status.

	Mean |SSE| in % (mean ± SD)	Max |SSE| in % (mean ± SD)
Inflammation status		
No inflammation ($n = 6$)	1.8 ± 0.2 ($N = 6$)	2.9 ± 0.5 ($N = 6$)
Medium level of inflammation ($n = 2$)	3.1 ± 0.2 ($N = 6$) (§: $p < 0.01$;†: $p < 0.001$)	4.5 ± 0.4 ($N = 6$) (§: $p < 0.01$;†: $p < 0.05$)
High level of inflammation ($n = 4$)	4.8 ± 0.4 ($N = 6$) (§: $p < 0.01$;†: $p < 0.001$)	5.6 ± 0.1 ($N = 7$) (§: $p < 0.01$;†: $p < 0.05$)

§: compared with no inflammation status.
†: compared with all other inflammation status.
N: required minimum population of patients for a 95% of confidence.

1) The stability of a vulnerable plaque is sensitive to small structural changes [61,62]. Therefore, the early detection of plaque instability and timely treatment to prevent myocardial infarctions may be provided with SSE imaging. However, this needs to be clinically validated afterward.
2) The ability to characterize material properties paves the road to clinical studies evaluating the performance of new drugs targeting on modifying plaque component mechanical properties (*e.g.*, rigidifying of the lipid core) for prevention of acute coronary events [15,54]. Mechanical properties of a plaque may be characterized more precisely if conventional elastograms are supplemented with SSE maps.
3) The inflammation status is a major determinant for the detection of vulnerable plaques [5]. We observed that high SSE is linked with plaque inflammation. In this regard, integration of SSE into the current clinical practice, once clinically validated, may help identifying patients who are at a higher risk and in need for closer follow-ups and further investigations. SSE may also improve risk stratification and facilitates clinical decision making.

Conflict of interest

The authors report no relationships that could be construed as a conflict of interest.

Acknowledgments

This research was supported by the Natural Sciences and Engineering Research Council of Canada (Collaborative Health Research program #323405-6 and International Strategic program #381136-09), and by the Canadian Institutes of Health Research (#CPG-80085). This research was also supported by a joint international program of the Agence Nationale de la Recherche of France (MELANII project #09-BLANC-0423). Dr. Zahra Keshavarz-Motamed was supported in part by a post-doctoral fellowship of the Fonds de la Recherche du Québec – Nature et Technologies (FQRNT).

Appendix

Elastography algorithm

LSME processes RF IVUS data in the polar coordinate system to estimate the strain tensor based on the detailed displacement field and its spatial derivative. To compensate for rigid motions of the catheter, RF images were first registered and overlapping measurement windows (MWs) within ROIs of two consecutive temporal images were analyzed. Subsequently, 2D correlation coefficients between the two images for each MW were calculated. Shifts of the maximum correlation point were taken as the motion of the catheter to be compensated in the second temporal image. Taylor series expansion of the optical flow equation in the polar coordinate system at each point of the MW around the centre of that window was written. This makes an over-determined system of equations in terms of the optical flow components and their partial spatial derivatives. This system of equations was solved in a least squares sense. The 2D-displacement gradient matrix (Δ) in the polar coordinate is defined as:

$$\Delta = \begin{bmatrix} \Delta_{rr} & \Delta_{r\theta} \\ \Delta_{\theta r} & \Delta_{\theta\theta} \end{bmatrix} = \begin{bmatrix} \dfrac{\partial U_r}{\partial r} & \dfrac{1}{r}\left(\dfrac{\partial U_r}{\partial \theta} - U_\theta\right) \\ \dfrac{\partial U_\theta}{\partial r} & \dfrac{1}{r}\left(\dfrac{\partial U_\theta}{\partial \theta} + U_r\right) \end{bmatrix} \tag{A1}$$

Components of the strain tensor in polar coordinates $\varepsilon_{ij} = \frac{1}{2}(\Delta_{ij} + \Delta_{ji})$ can be calculated as:

$$\varepsilon = \begin{bmatrix} \varepsilon_{rr} & \varepsilon_{r\theta} \\ \varepsilon_{\theta r} & \varepsilon_{\theta\theta} \end{bmatrix} = \begin{bmatrix} \Delta_{rr} & \dfrac{1}{2}(\Delta_{r\theta} + \Delta_{\theta r}) \\ \dfrac{1}{2}(\Delta_{r\theta} + \Delta_{\theta r}) & \Delta_{\theta\theta} \end{bmatrix} \tag{A2}$$

where Δ, ε and U are the displacement gradient tensor, the strain tensor and the displacement vector, respectively. Reported SSE corresponds to $\Delta_{r\theta}$, as further explained in Ref. [39].

Another issue limiting the performance of IVUS elastography is the eccentricity of the catheter within the vessel lumen, due to the pulsatile flow and cardiac motion, potentially leading to erroneous strain estimates. The method used to estimate the eccentricity and to correct strain estimates in the polar coordinate system is also detailed with complete equations elsewhere [39]. In this study, sizes of 2D MWs were 120 × 30 pixels (0.924 mm × 0.369 radian), with 90% radial and circumferential overlaps. The size of each RF image was 800 × 512 pixels. Shear strain elastograms (SSE) were computed and analyzed during diastole, and smoothed using a 5 × 5 pixels median filter padded with symmetric expansion at the boundaries. The timing within each cardiac cycle was the same pre- and post-DCA.

References

[1] Virmani R, Kolodgie FD, Burke AP, Farb A, Schwartz SM. Lessons from sudden coronary death: a comprehensive morphological classification scheme for atherosclerotic lesions. Arterioscler Thromb Vasc Biol 2000;20:1262–75.
[2] Tabas I. Apoptosis and plaque destabilization in atherosclerosis: the role of macrophage apoptosis induced by cholesterol. Cell Death Differ 2004;11:S12–6.
[3] Virmani R, Burke AP, Farb A, Kolodgie FD. Pathology of the vulnerable plaque. Am J Cardiol 2006;47:13–8.
[4] Fleg JM, Stone GW, Fayad ZA, Granada JF, Hatsukami TS, Kolodgie FD, et al. Detection of high-risk atherosclerotic plaque report of the NHLBI working group on current status and future directions. JACC Cardiovasc Imaging 2012;5:941–55.
[5] Naghavi M, Libby P, Falk E, Casscells SW, Litovsky S, Rumberger J, et al. From vulnerable plaque to vulnerable patient: a call for new definition and risk assessment strategies: part I. Circulation 2003;108:1664–72.
[6] Rioufol G, Finet G, Ginon I, Andre-Fouet X, Rossi R, Vialle E, et al. Multiple atherosclerotic plaque rupture in acute coronary syndrome: a three-vessel intravascular ultrasound study. Circulation 2002;106:804–8.
[7] Carlier SG, Tanaka K. Studying coronary plaque regression with IVUS: a critical review of recent studies. J Interv Cardiol 2006;19:11–5.
[8] Tardif JC, Lesage F, Harel F, Romeo P, Pressacco J. Imaging biomarkers in atherosclerosis trials. Circ Cardiovasc Imaging 2011;4:319–33.
[9] Jang IK, Bouma BE, Kang DH, Park SJ, Park SW, Seung KB, et al. Visualization of coronary atherosclerotic plaques in patients using optical coherence tomography: comparison with intravascular ultrasound. J Am Coll Cardiol 2002;39:604–9.
[10] Tearney GJ, Waxman S, Shishkov M, Vakoc BJ, Suter MJ, Freilich MI, et al. Three-dimensional coronary artery microscopy by intracoronary optical frequency domain imaging. JACC Cardiovasc Imaging 2008;1:752–61.
[11] Fayad ZA, Fuster V, Nikolaou K, Becker C. Computed tomography and magnetic resonance imaging for noninvasive coronary angiography and plaque imaging: current and potential future concepts. Circulation 2002;106:2026–34.
[12] Briley-Saebo KC, Mulder WJ, Mani V, Hyafil F, Amirbekian V, Aguinaldo JG, et al. Magnetic resonance imaging of vulnerable atherosclerotic plaques: current imaging strategies and molecular imaging probes. J Magn Reason Imaging 2007;26:460–79.
[13] Loree HM, Kamm RD, Stringfellow RG, Lee RT. Effects of fibrous cap thickness on peak circumferential stress in model atherosclerotic vessels. Circ Res 1992;71:850–8.
[14] Ohayon J, Finet G, Gharib AM, Herzka DA, Tracqui P, Heroux J, et al. Necrotic core thickness and positive arterial remodeling index: emergent biomechanical factors for evaluating the risk of plaque rupture. Am J Physiol Heart Circ Physiol 2008;295:717–27.
[15] Finet G, Ohayon J, Rioufol G. Biomechanical interaction between cap thickness, lipid core composition and blood pressure in vulnerable coronary plaque: impact on stability or instability. Coron Artery Dis 2004;15:13–20.
[16] de Korte CL, Pasterkamp G, van der Steen AFW, Woutman HA, Bom N. Characterization of plaque components with intravascular ultrasound

elastography in human femoral and coronary arteries *in vitro*. Circulation 2000;102:617–23.
[17] de Korte CL, Sierevogel MJ, Mastik F, Strijder C, Schaar JA, Velema E, et al. Identification of atherosclerotic plaque components with intravascular ultrasound elastography *in vivo*: a Yucatan pig study. Circulation 2002;105:1627–30.
[18] Céspedes EI, de Korte CL, van der Steen AFW. Intraluminal ultrasonic palpation: assessment of local and cross-sectional tissue stiffness. Ultrasound Med Biol 2000;26:385–96.
[19] Schaar JA, van der Steen AF, Mastik F, Baldewsing RA, Serruys PW. Intravascular palpography for vulnerable plaque assessment. J Am Coll Cardiol 2006;18:86–91.
[20] Nair A, Kuban BD, Tuzcu EM, Schoenhagen P, Nissen SE, Vince DG. Coronary plaque classification with intravascular ultrasound radiofrequency data analysis. Circulation 2002;106:2200–6.
[21] Nair A, Margolis MP, Kuban BD, Vince DG. Automated coronary plaque characterization with intravascular ultrasound backscatter: *ex vivo* validation. Euro-Interv 2007;3:113–20.
[22] Frutkin AD, Mehta SK, McCrary JR, Marso SP. Limitations to the use of virtual histology-intravascular ultrasound to detect vulnerable plaque. Eur Heart J 2007;28:1783–4.
[23] Thim T, Hagensen MK, Wallace-Bradley D, Granada JF, Kaluza GL, Drouet L, et al. Unreliable assessment of necrotic core by virtual histology intravascular ultrasound in porcine coronary artery disease. Circ Cardiovasc Imaging 2010;3:384–91.
[24] Brugaletta S, Garcia-Garcia HM, Serruys PW, Maehara A, Farooq V, Mintz GS, et al. Relationship between palpography and virtual histology in patients with acute coronary syndromes. JACC Cardiovasc Imaging 2012;5:19–27.
[25] Maehara A, Cristea E, Mintz GS, Lansky AJ, Dressler O, Biro S, et al. Definitions and methodology for the grayscale and radiofrequency intravascular ultrasound and coronary angiographic analyses. JACC Cardiovasc Imaging 2012;5:1–9.
[26] Murray SW, Stables RH, Hart G, Palmer ND. Defining the magnitude of measurement variability in the virtual histology analysis of acute coronary syndrome plaques. Eur Heart J Cardiovasc Imaging 2013;14:167–74.
[27] Cinthio M, Ahlgren AR, Bergkvist J, Jansson T, Persson HW, LindstrÖm K. Longitudinal movements and resulting shear strain of the arterial wall. Am J Physiol Heart Circ Physiol 2006;291:394–402.
[28] Idzenga T, Pasterkamp G, de Korte CL. Shear strain in the adventitial layer of the arterial wall facilitates development of vulnerable plaques. Biosci Hypotheses 2009;2:339–42.
[29] Idzenga T, Holewijn S, Hansen HHG, de Korte CL. Estimating cyclic shear strain in the common carotid artery using radiofrequency ultrasound. Ultrasound Med Biol 2012;38:2229–37.
[30] Lawrence-Brown M, Stanley BM, Sun Z, Semmens JB, Liffman K. Stress and strain behaviour modelling of the carotid bifurcation. ANZ J Surg 2011;81:810–6.
[31] Vito RP, Whang MC, Giddens DP, Zarins CK, Glagov S. Stress analysis of the diseased arterial cross-section. ASME Adv Bioeng Proc 1990;19:273–6.
[32] Falk E, Shah PK, Fuster V. Coronary plaque disruption. Circulation 1995;92:657–71.
[33] Dickson BC, Gotlieb AI. Towards understanding acute destabilization of vulnerable atherosclerotic plaques. Cardiovasc Pathol 2003;12:237–48.
[34] de Korte CL, van der Steen AF, Céspedes EI, Pasterkamp G. Intravascular ultrasound elastography in human arteries: initial experience *in vitro*. Ultrasound Med Biol 1998;24:401–8.
[35] Wan M, Li Y, Li J, Cui Y, Zhou X. Strain imaging and elasticity reconstruction of arteries based on intravascular ultrasound video images. IEEE Trans Biomed Eng 2001;48:116–20.
[36] Maurice RL, Fromageau J, Roy Cardinal MH, Doyley M, de Muinck E, Robb J, et al. Characterization of atherosclerotic plaques and mural thrombi with intravascular ultrasound elastography: a potential method evaluated in an aortic rabbit model and a human coronary artery. IEEE Trans Inf Technol Biomed 2008;12:290–8.
[37] Liang Y, Zhu H, Friedman MH. Estimation of the transverse strain tensor in the arterial wall using IVUS image registration. Ultrasound Med Biol 2008;34:1832–45.
[38] Maurice RL, Ohayon J, Finet G, Cloutier G. Adapting the Lagrangian speckle model estimator for endovascular elastography: theory and validation with simulated radio-frequency data. J Acoust Soc Am 2004;116:1276–86.
[39] Majdouline Y, Ohayon J, Keshavarz-Motamed Z, Roy Cardinal MH, Garcia D, Allard L, et al. Endovascular shear strain elastography for the detection and characterization of the severity of atherosclerotic plaques: *in vitro* validation and *in vivo* evaluation. Ultrasound Med Biol 2014;40(5):890–903.
[40] Soulez G, Lerouge S, Allard L, Roméo P, Qi S, Héon H, et al. Vulnerable carotid atherosclerotic plaque creation in a swine model: evaluation of stenosis creation using absorbable and permanent suture in a diabetic dyslipidemic model. J Vasc Interv Radiol 2012;23:1700–8.
[41] Saijo Y, Tanaka A, Iwamoto T, Filho EDS, Yoshizawa M, Hirosaka A, et al. Intravascular two-dimensional tissue strain imaging. Ultrasonics 2006;44:147–51.
[42] Le Floc'h S, Cloutier G, Sajio Y, Finet G, Yazdani SK, Deleaval F, et al. A four criterion selection procedure for atherosclerotic plaque elasticity reconstruction based on *in vivo* coronary intravascular ultrasound radial strain sequences. Ultrasound Med Biol 2012;38:2084–97.
[43] Solem J, Levin M, Karlsson T, Grip L, Albertsson P, Wiklund O. Composition of coronary plaques obtained by directional atherectomy in stable angina: its relation to serum lipids and statin treatment. J Intern Med 2006;259:267–75.
[44] Kimura S, Yonetsu T, Suzuki K, Isobe M, Iesaka Y, Kakuta T. Characterisation of non-calcified coronary plaque by 16-slice multidetector computed tomography: comparison with histopathological specimens obtained by directional coronary atherectomy. Int J Cardiovasc Imaging 2012;28:1749–62.
[45] Lee RT, Grodzinsky AJ, Frank EH, Kamm RD, Schoen FJ. Structure-dependent dynamic mechanical behavior of fibrous caps from human atherosclerotic plaques. Circulation 1991;83:1764–70.
[46] Loree HM, Tobias BJ, Gibson LJ, Kamm RD, Small DM, Lee RT. Mechanical properties of model atherosclerotic lesion lipid pools. Arterioscler Thromb 1994;14:230–4.
[47] Williamson SD, Lam Y, Younis HF, Huang H, Patel S, Kaazempur-Mofrad MR, et al. On the sensitivity of wall stresses in diseased arteries to variable material properties. J Biomech Eng 2003;125:147–55.
[48] Tracqui P, Broisat A, Toczek J, Mesnier N, Ohayon J, Riou L. Mapping elasticity moduli of atherosclerotic plaque in situ via atomic force microscopy. J Struct Biol 2011;174:115–23.
[49] Hayenga HN, Trache A, Trzeciakowski J, Humphrey JD. Regional atherosclerotic plaque properties in ApoE-/- mice quantified by atomic force, immunofluorescence, and light microscopy. J Vasc Res 2011;48:495–504.
[50] Destrempes F, Roy Cardinal MH, Allard L, Tardif JC, Cloutier G. Segmentation method of intravascular ultrasound images of human coronary arteries. Comput Med Imaging Graph 2014;38(2):91–103.
[51] Lee RT, Loree HM, Cheng GC, Lieberman EH, Jaramillo N, Schoen FJ. Computational structural analysis based on intravascular ultrasound imaging before *in vitro* angioplasty: prediction of plaque fracture locations. J Am Coll Cardiol 1993;21:777–82.
[52] Fayad ZA, Fuster V. Clinical imaging of the high-risk or vulnerable atherosclerotic plaque. Circ Res 2001;89:305–16.
[53] Kips JG, Segers P, Van Bortel LM. Identifying the vulnerable plaque: a review of invasive and non-invasive imaging modalities. Artery Res 2008;2:21–34.
[54] Cheng GC, Loree HM, Kamm RD, Fishbein MC, Lee RT. Distribution of circumferential stress in ruptured and stable atherosclerotic lesions. A structural analysis with histopathological correlation. Circulation 1993;87:1179–87.
[55] Suh WM, Seto AH, Margey RJP, Cruz-Gonzalez I, Jang IK. Intravascular detection of the vulnerable plaque. Circ Cardiovasc Imaging 2011;4:169–78.
[56] Arroyo LH, Lee RT. Mechanisms of plaque rupture: mechanical and biologic interactions. Cardiovasc Res 1999;41:369–75.
[57] van der Wal AC, Becker AE, van der Loos CM, Das PK. Site of intimal rupture or erosion of thrombosed coronary atherosclerotic plaques is characterized by an inflammatory process irrespective of the dominant plaque morphology. Circulation 1994;89:36–44.
[58] Libby P, Ridker PM, Maseri A. Inflammation and atherosclerosis. Circulation 2002;105:1135–43.
[59] Burke AP, Kolodgie FD, Farb A, Weber D, Virmani R. Morphological predictors of arterial remodeling in coronary atherosclerosis. Circulation 2002;105:297–303.
[60] Bhatia V, Bhatia R, Dhindsa S, Virk A. Vulnerable plaques, inflammation and newer imaging modalities. J Postgrad Med 2003;49:361–8.
[61] Libby P. Current concepts of the pathogenesis of the acute coronary syndromes. Circulation 2001;104:365–72.
[62] Le Floc'h S, Cloutier G, Finet G, Tracqui P, Pettigrew RI, Ohayon J. On the potential of a new IVUS elasticity modulus imaging approach for detecting vulnerable atherosclerotic coronary plaques: *in vitro* vessel phantom study. Phys Med Biol 2010;55:5701–21.